Supplementary Information

Dynamics within the CD95 Death-Inducing Signaling Complex Decide Life and Death of Cells

Leo Neumann, Carina Pforr, Joel Beaudouin, Alexander Golks, Nicolai Fricker, Peter H. Krammer, Inna N. Lavrik, Roland Eils

Table of Contents

Table S1	Model definition
Table S2	Model parameters
Figure S1	Apoptosis induction in HeLa-CD95 cells
Figure S2	Simulation of complete model
Figure S3	CD95 DISC-Immunoprecipitation
Figure S4	Apoptotic and NF-κB signaling diverge at the DISC
Figure S5 A-G	Reduced models
Figure S6	Comparison of confidence interval size
Figure S7	Apoptosis in cells with downregulated c-FLIP
Figure S8	NF-κB activation in cells with downregulated c-FLIP
Figure S9	Impaired c-FLIP$_L$ processing

Table S1. Model definition

The table lists the reaction rates and the differential equations derived from the uni- or bimolecular reactions depicted in Figure 5A using the law-of-mass-action. In the diagram the DISC configurations not leading to further signaling were grouped in one entity marked L·RF·X·X. Here instead, we model all DISC configuration separately to keep track accurately of procaspase-8 amounts in parameter estimation.

Reaction Rates	Differential Equations	
$v_1 = k_1 \cdot [L] \cdot [RF]$	$d[L]/dt = -v_1$	(1)
$v_2 = k_2 \cdot [L{\cdot}RF] \cdot [C8]$	$d[L{\cdot}RF]/dt = v_1-v_2-v_3-v_4$	(2)
$v_3 = k_3 \cdot [L{\cdot}RF] \cdot [FL]$	$d[L{\cdot}RF{\cdot}C8]/dt = v_2-v_5-v_6-v_7$	(3)
$v_4 = k_4 \cdot [L{\cdot}RF] \cdot [FS]$	$d[L{\cdot}RF{\cdot}FL]/dt = v_3-v_8-v_9-v_{10}$	(4)
$v_5 = k_5 \cdot [L{\cdot}RF{\cdot}C8] \cdot [C8]$	$d[L{\cdot}RF{\cdot}FS]/dt = v_4-v_{11}-v_{12}-v_{13}$	(5)
$v_6 = k_6 \cdot [L{\cdot}RF{\cdot}C8] \cdot [FL]$	$d[p43/p41]/dt = 2{\cdot}v_5-2{\cdot}v_{14}+v_{16}$	(6)
$v_7 = k_7 \cdot [L{\cdot}RF{\cdot}C8] \cdot [FS]$	$d[C3]/dt = -v_{15}$	(7)
$v_8 = k_5 \cdot [L{\cdot}RF{\cdot}FL] \cdot [C8]$	$d[C8]/dt = -v_2-v_5-v_8-v_{11}-v_{16}$	(8)
$v_9 = k_6 \cdot [L{\cdot}RF{\cdot}FL] \cdot [FL]$	$d[C8^*]/dt = v_{14}-v_{17}$	(9)
$v_{10} = k_7 \cdot [L{\cdot}RF{\cdot}FL] \cdot [FS]$	$d[C3^*]/dt = v_{15}-v_{18}$	(10)
$v_{11} = k_5 \cdot [L{\cdot}RF{\cdot}FS] \cdot [C8]$	$d[p43\text{-}FLIP]/dt = v_6+v_8-v_{19}$	(11)
$v_{12} = k_6 \cdot [L{\cdot}RF{\cdot}FS] \cdot [FL]$	$d[NF\text{-}\kappa B{\cdot}I\kappa B]/dt = -v_{20}$	(12)
$v_{13} = k_7 \cdot [L{\cdot}RF{\cdot}FS] \cdot [FS]$	$d[NF\text{-}\kappa B{\cdot}I\kappa B{\cdot}P]/dt = v_{20}-v_{21}$	(13)
$v_{14} = k_8 \cdot [p43/p41] \cdot [p43/p41]$	$d[p43\text{-}FLIP{\cdot}IKK^*])/dt = v_{19}-v_{22}$	(14)
$v_{15} = k_9 \cdot [C3] \cdot [C8^*]$	$d[NF\text{-}\kappa B^*]/dt = v_{21}-v_{23}$	(15)
$v_{16} = k_{10} \cdot [C8] \cdot [C3^*]$	$d[RF]/dt = -v_1$	(16)
$v_{17} = k_{11} \cdot [C8^*]$	$d[FL]/dt = -v_3-v_6-v_9-v_{12}$	(17)
$v_{18} = k_{12} \cdot [C3^*]$	$d[FS]/dt = -v_4-v_7-v_{10}-v_{13}$	(18)
$v_{19} = k_{13} \cdot [p43\text{-}FLIP] \cdot [IKK]$	$d[IKK]/dt = -v_{19}$	(19)
$v_{20} = k_{14} \cdot [NF\text{-}\kappa B{\cdot}I\kappa B] \cdot [p43\text{-}FLIP{\cdot}IKK^*]$	$d[L{\cdot}RF{\cdot}C8{\cdot}FS]/dt = v_7+v_{11}$	(20)
$v_{21} = k_{15} \cdot [NF\text{-}\kappa B{\cdot}I\kappa B{\cdot}P]$	$d[L{\cdot}RF{\cdot}FL{\cdot}FL]/dt = v_9$	(21)
$v_{22} = k_{16} \cdot [p43\text{-}FLIP{\cdot}IKK^*]$	$d[L{\cdot}RF{\cdot}FL{\cdot}FS]/dt = v_{10}+v_{12}$	(22)
$v_{23} = k_{17} \cdot [NF\text{-}\kappa B^*]$	$d[L{\cdot}RF{\cdot}FS{\cdot}FS]/dt = v_{13}$	(23)

Table S2. Model parameters

The table lists the reaction constants and initial concentrations used in the model. The values of the reaction constants were obtained by parameter estimation. Initial concentrations were either estimated from the data, assumed to be zero or derived directly in the case of the anti-CD95 antibodies.

Parameter	Value	Unit	Comment
k_1	1.0000e+00	$nMol^{-1}\,min^{-1}$	Binding of ligand to receptor
k_2	1.2772e-04	$nMol^{-1}\,min^{-1}$	1. binding of C8 to DISC
k_3	6.6933e-01	$nMol^{-1}\,min^{-1}$	1. binding of FL to DISC
k_4	1.0000e-05	$nMol^{-1}\,min^{-1}$	1. binding of FS to DISC
k_5	5.9466e-04	$nMol^{-1}\,min^{-1}$	2. binding of C8 to DISC
k_6	1.0000e+00	$nMol^{-1}\,min^{-1}$	2. binding of FL to DISC
k_7	8.8751e-01	$nMol^{-1}\,min^{-1}$	2. binding of FS to DISC
k_8	8.0444e-04	$nMol^{-1}\,min^{-1}$	Processing of p43/p41 to C8
k_9	2.2498e-03	$nMol^{-1}\,min^{-1}$	Processing of C3 to C3* by C8*
k_{10}	1.2053e-01	$nMol^{-1}\,min^{-1}$	Processing of C8 to p43/p41 by C3*
k_{11}	2.8915e-02	min^{-1}	Degradation of C8*
k_{12}	1.5029e-01	min^{-1}	Degradation of C3*
k_{13}	7.2043e-04	$nMol^{-1}\,min^{-1}$	Binding of p43-FLIP to IKK
k_{14}	3.5882e-01	$nMol^{-1}\,min^{-1}$	Phosphoryl. of NF-κB·IκB by p43-FLIP·IKK*
k_{15}	3.6842e+00	min^{-1}	Activation of NF-κB*
k_{16}	2.2299e-02	min^{-1}	Degradation of p43-FLIP·IKK*
k_{17}	6.4182e-03	min^{-1}	Degradation of NF-κB*
$[L]_0$	1.1322e+02	nM	Initial conc. of anti-CD95 (1500 ng/ml)
$[L]_0$	3.7740e+01	nM	Initial conc. of anti-CD95 (500 ng/ml)
$[L]_0$	1.8870e+01	nM	Initial conc. of anti-CD95 (250 ng/ml)
$[C3]_0$	1.4434e+00	nM	Initial conc. of procaspase-3
$[C8]_0$	6.4477e+01	nM	Initial conc. of procaspase-8
$[NF\text{-}\kappa B\cdot I\kappa B]_0$	4.7395e+00	nM	Initial conc. of NF-κB·IκB
$[RF]_0$	9.1266e+01	nM	Initial conc. of CD95-FADD entity
$[FL]_0$	7.3986e+00	nM	Initial conc. of c-$FLIP_L$
$[FS]_0$	5.0839e+00	nM	Initial conc. of c-$FLIP_S$
$[IKK]_0$	5.7728e+00	nM	Initial conc. of inactive IKK
other	0.0000e+00	nM	Initial conc. of all other molecules

Figure S1. Apoptosis induction in HeLa-CD95 cells

Specific apoptosis was assessed in HeLa-CD95 cells at various concentrations of anti-CD95 antibodies and incubation periods. Cell death was examined by analyzing DNA fragmentation. Cells were lysed in buffer containing 0,1% (w/v) sodium citrate, 0,2% (v/v) Nonidet P40 (Roche), 50 μg/ml propidium iodide (Sigma). After incubation at 37°C in the dark for 30 min nuclei were quantified by FACScan (Becton Dickinson).

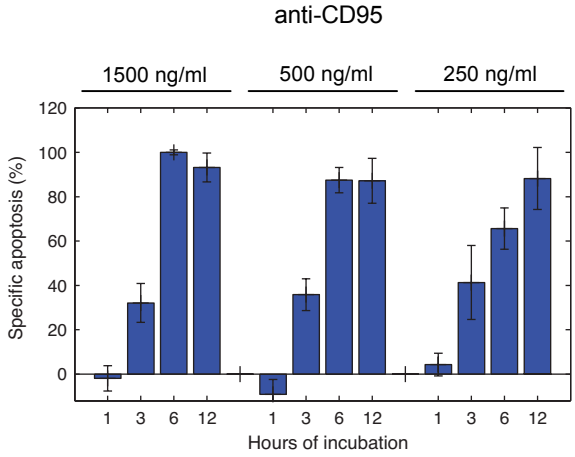

Figure S2. Simulation of complete model

The panels show the simulated concentration of given proteins in HeLa-CD95 cells using the complete model depicted in Figure 3. Proteins labeled '(sum)' are observables obtained by summing stochiometrically over all variables corresponding to complexes containing the protein of interest e.g. C3* (sum) = C3* + IAP·C3* + C6·C3*. Black, blue and red colors correspond to 1500, 500 and 250 ng/ml anti-CD95 used to induce the cells at time t = 0. Squares, diamonds and triangles indicate experimental data obtained by western blot (cf. Fig. 2).

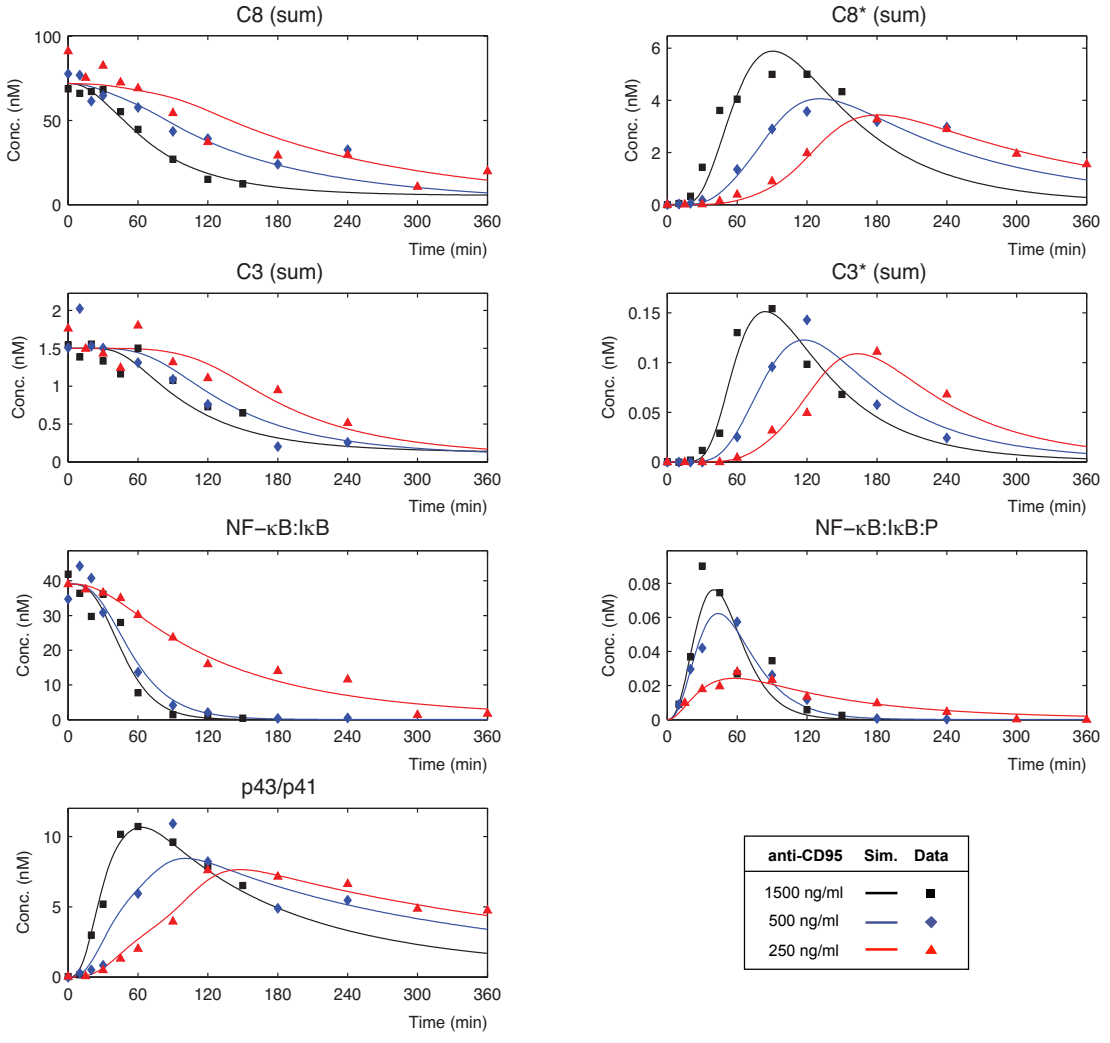

Figure S3. CD95 DISC-Immunoprecipitation

HeLa-CD95 cells were kept under non-stimulated conditions for control (anti-CD95 -) or stimulated with 500 ng/ml anti-CD95 for 30 min (anti-CD95 +). The lysates were used for a CD95 DISC-IP. Therefore, anti-CD95 was added to untreated and treated lysates in order to immunoprecipitate. The immunoprecipitated proteins (CD95-IP) and the corresponding lysates (Lysate) were analyzed by western blots using antibodies against caspase-8, IKKa/b and CD95.

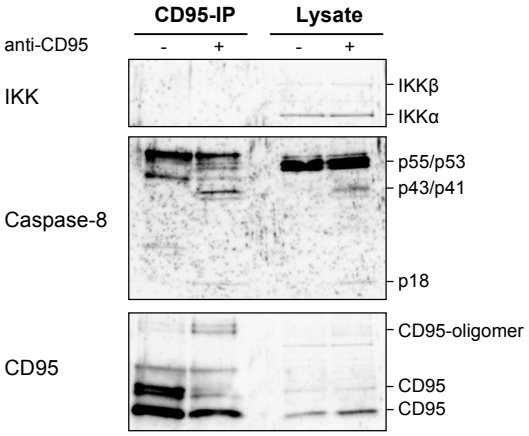

Figure S4. Apoptotic and NF-κB signaling diverge at the DISC

(A) HeLa-CD95 cells expressing p65-mCherry were treated with zVAD-fmk for 30 minutes, then induced with 250 ng/ml of anti-CD95 and imaged by confocal laser scanning microscopy over the indicated time interval. Measurements of mCherry (depicted in gray) indicated translocation of p65 upon CD95 activation. Scale bar: 10 μm.

(B) Hela-CD95 cells were treated with zVAD-fmk for 30 minutes, then induced with 250 ng/ml of anti-CD95. Total cellular lysates were analyzed by western blots using antibodies against caspase-8, p-IκBα, c-FLIP and tubulin.

A

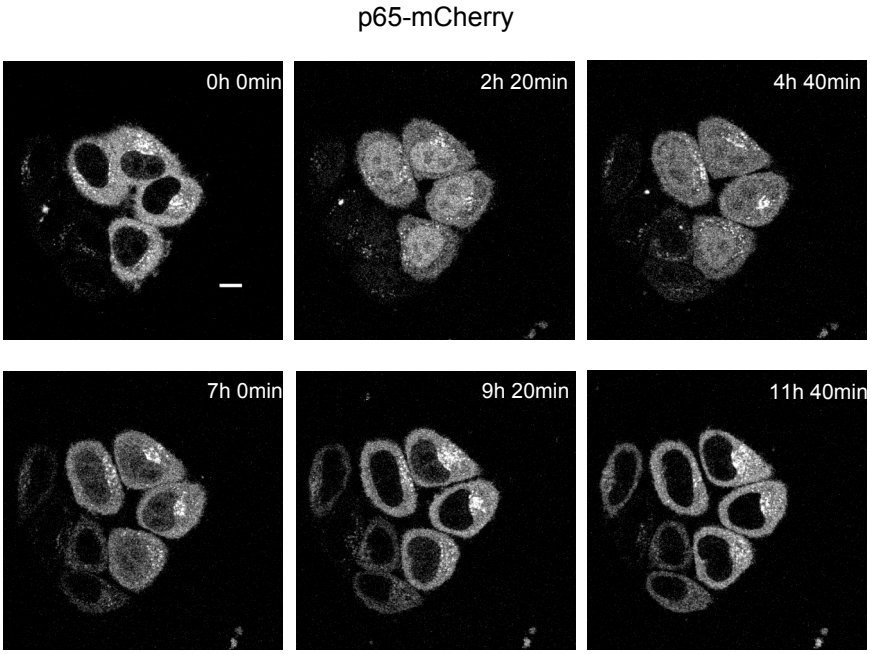

B

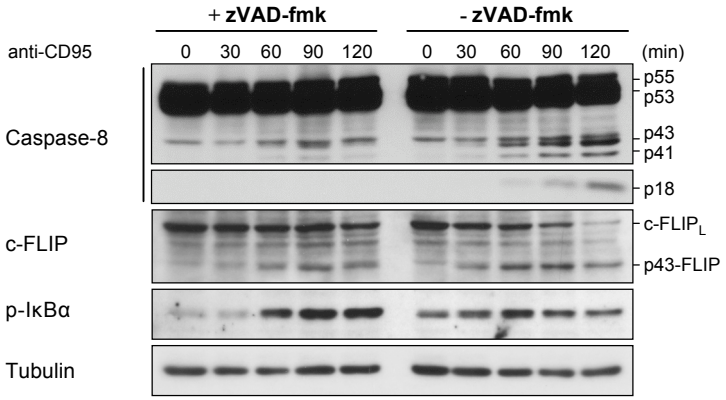

Figure S5A. Model two

The diagram depicts model two which is obtained by simplifying the complete model. We sought for a way to reduce the description of DISC formation and regarded the trimerization of FADD (F) to be a potentially inessential reaction step in terms of model dynamics. Hence, it was assumed that FADD is already in trimeric form. This modification decreased massively the number of reactions of the model (from 92 to 61).

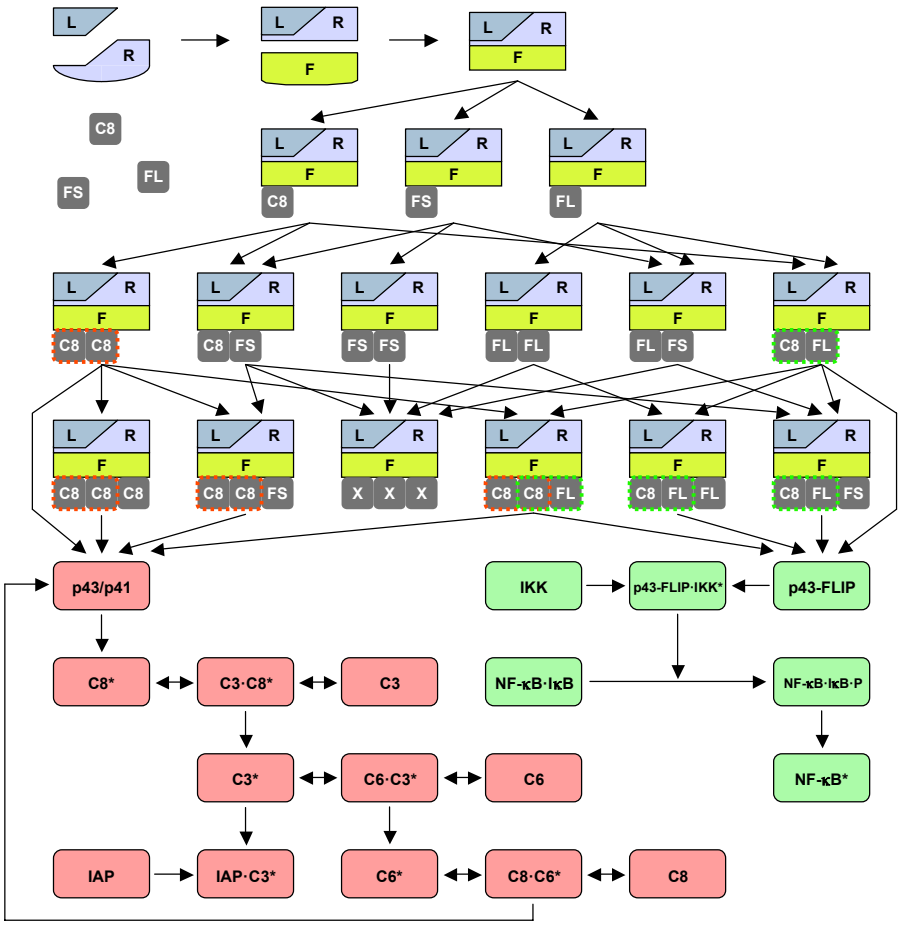

Figure S5B. Model three

To further simplify the DISC assembly we considered that the adaptor protein FADD is merely an additional step in the linear chain of early DISC formation in model two. The third model was obtained by merging the CD95 receptor (R) and FADD (F) into one species denoted by RF. In our simulations, we did not observe any differences in the dynamical features of the model in comparison to model two given different sets of parameters (data not shown). The number of reactions was reduced from 61 to 60.

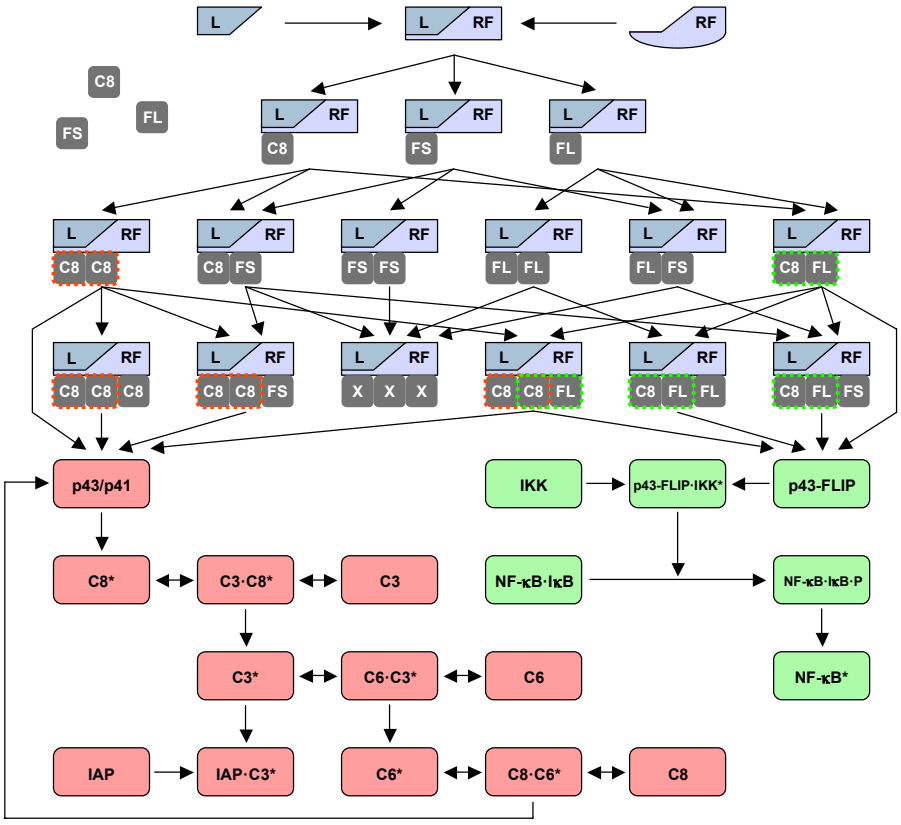

Figure S5C. Model four

To further reduced the model we turned our attention to the apoptotic feedback loop. Although caspase-6 is known to engage in CD95-mediated apoptosis we did not have any data for it. We wondered if we could reproduce the activation dynamics of caspase-8 and -3 if we removed caspase-6 from the apoptotic feedback loop. We observed a 2.76% decrease in the normalized goodness-of-fit and regarded caspase-6 to be dispensable for our study, as our focus was rather the assembly of the DISC and the divergence of apoptotic and NF-κB signaling. In this reduction step the number of reactions fell from 60 to 56.

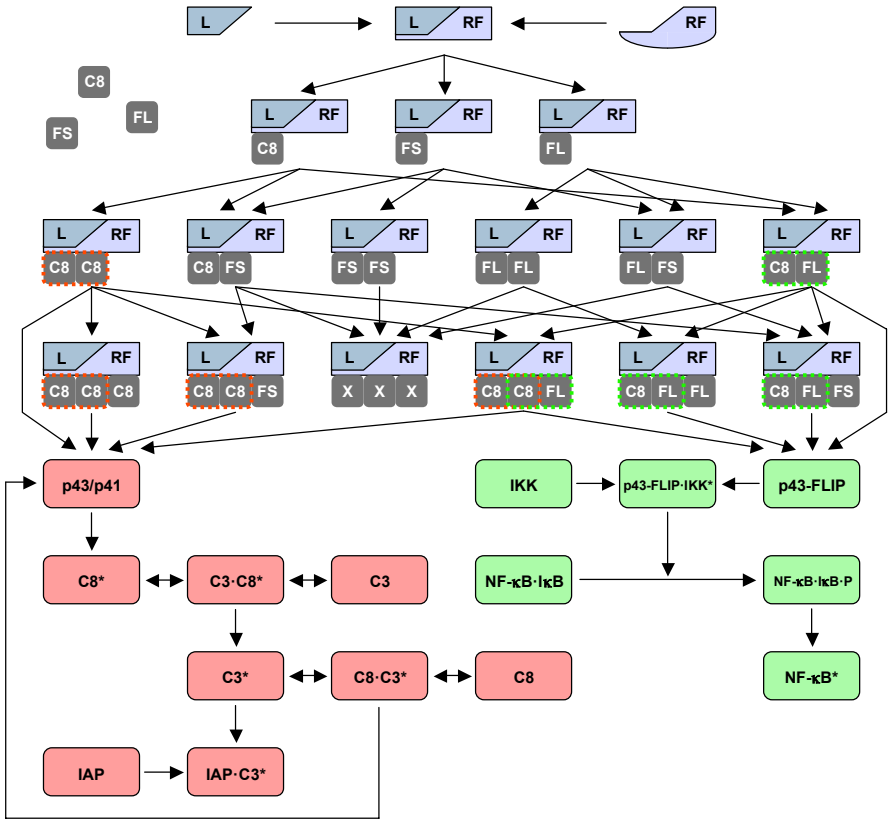

Figure S5D. Model five

Up to model four the process of caspase activation was modeled with the reaction scheme S+E ↔ S·E → P+E (S=substrate, E=enzyme and P=product). In model five it was simplified to S+E → P+E, thereby further reducing the number of reactions (from 56 to 51). We expected a sharp drop in the ability of the model to fit the experimental data set. Surprisingly, the decrease of the normalized fit measured only 2.25%, thus justifying the reduction step. It should be noted, however, that this result might be facilitated partially by the fact that we used cell population data, which typically shows smoothed activation curves as compared to single cell dynamics.

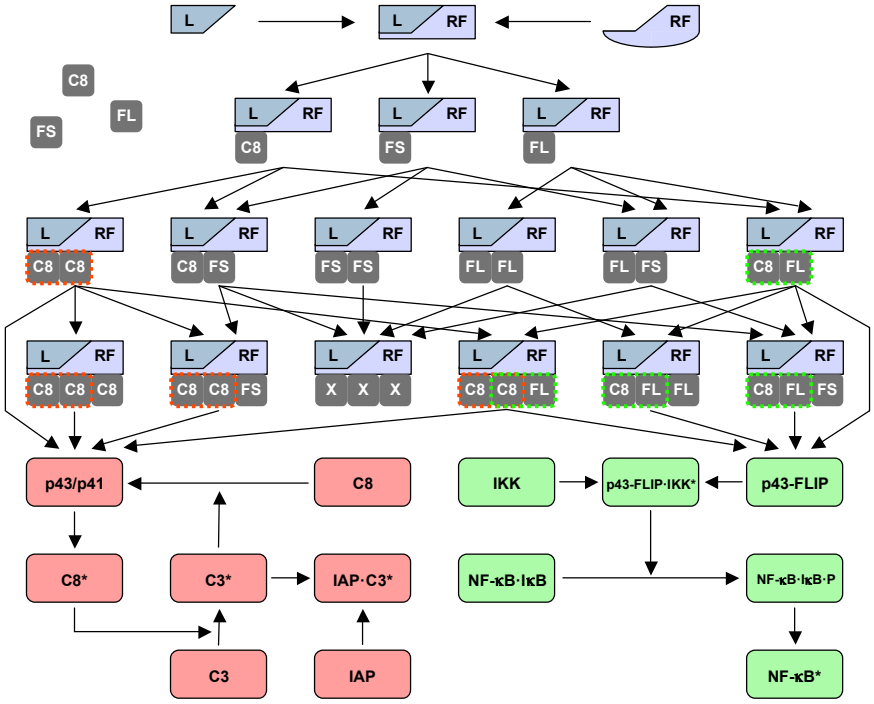

Figure S5E. Model six

To further simplify DISC assembly we considered that p43/p41 can be formed when the DISC is occupied only with two copies of procaspase-8. Analogously, p43-FLIP can be generated already when one copy of procaspase-8 and one copy of c-FLIP$_L$ are present. Hence, we omitted all triple DISC configurations (e.g. L·RF·C8·C8·FS). DISC configuration, which do not lead to further signaling, were pooled in the entity denoted by X·X for the sake of concise display. This reduction step lowered drastically the number of reactions from 51 to 27.

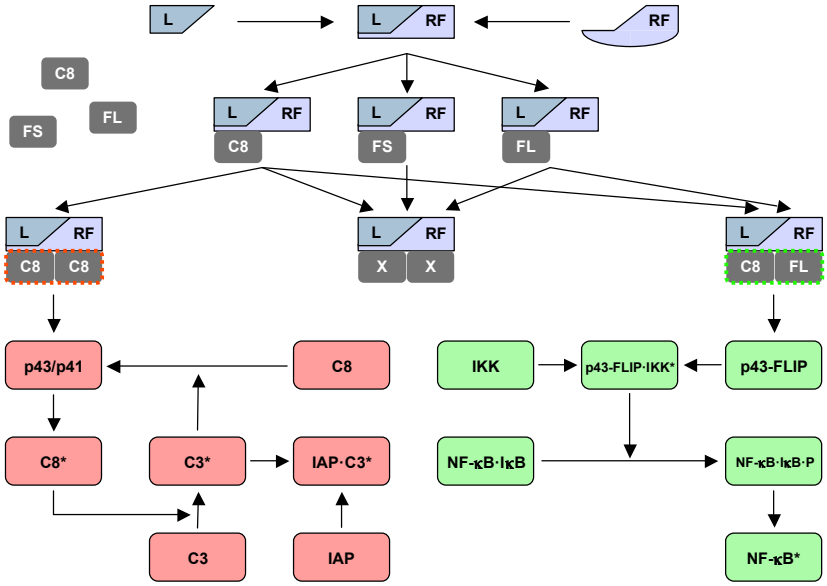

Figure S5F. Model seven

To further simplify the model, we considered the linear reaction chains of p43/p41 and p43-FLIP generation. We merged the two steps into a one-step reaction by omitting the entities L·RF·C8·C8 and L·RF·C8·FL, thus obtaining a minimal model of DISC formation. The number of reactions decreased from 27 to 25.

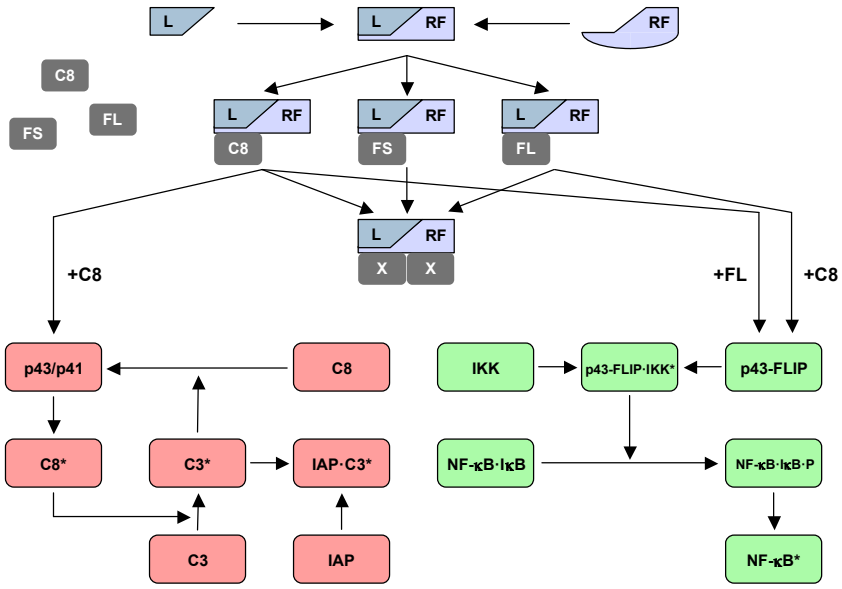

Figure S5G. Model eight (*Reduced Model*)

Model eight was obtained simply by taking away the inhibition of caspase-3 by IAP. Although IAP's role of caspase inhibition is undisputed, it did not seem to play an important role in our setting, as shown by the good model fit to caspase-3 data. The number of reactions fell from 25 to 23 with respect to model seven. Model eight was used for further prediction in our study as it displayed the best trade-off between model complexity and ability to reproduce the experimental observations.

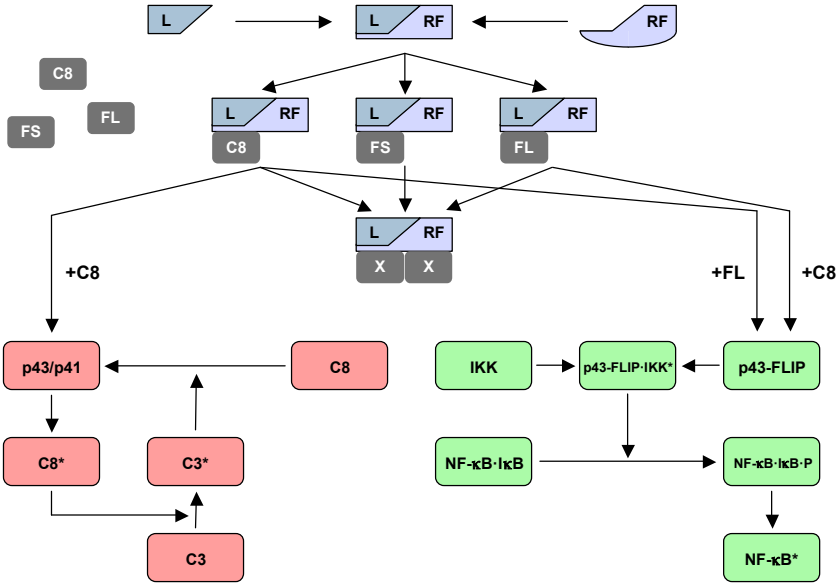

Figure S6. Comparison of confidence interval size

For every parameter p of the models one to eight we calculated the 95% confidence interval $CI = [\, p\text{-}d, p\text{+}d \,]$ using MATLAB's `nlparci` function. We measured the normalized size z of the confidence interval by defining $z = 2(p\text{+}d)/p$. The histogram displays the relative frequency of the logarithm of z for the different models. The complete model (dark red) exhibits many large confidence intervals of up to 13 orders of magnitude whereas for the reduced model (dark blue) most sizes lie within one or two orders.

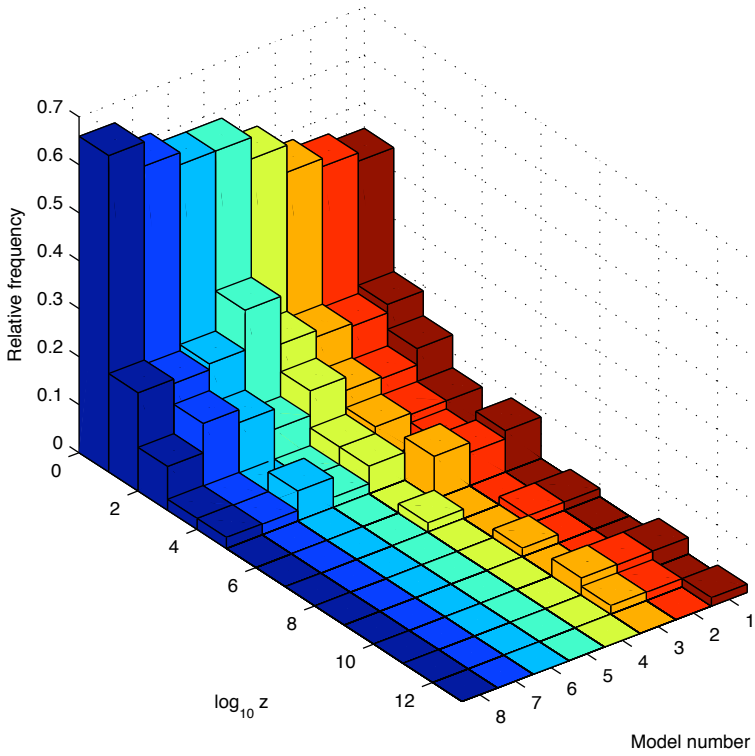

Figure S7. Apoptosis in cells with downregulated c-FLIP

Cell death assay of HeLa-CD95 cells with c-FLIP$_L$ downregulation in comparison to control transfected cells (control). Shown is specific apoptosis normalized to 100% for HeLa-CD95 cells (control). Cells were treated with the depicted amount of anti-CD95 for 18h. Cell death was determined with PI staining and analyzed with flow cytometry. Specific cell death was calculated as described in Materials and methods.

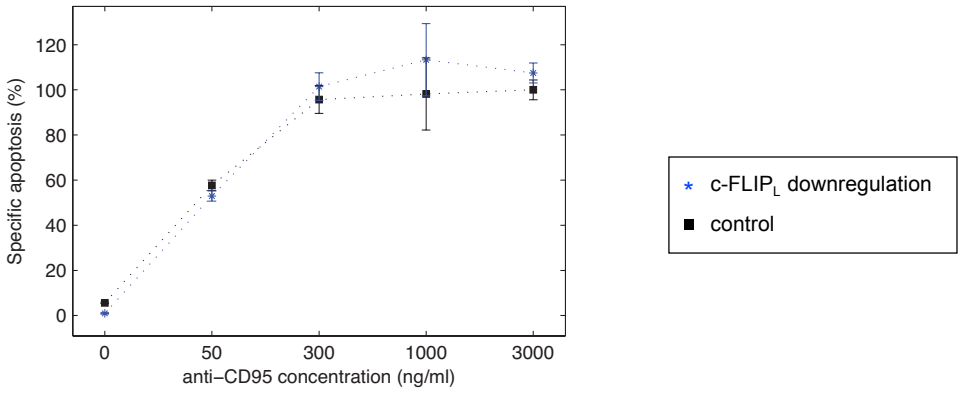

Figure S8. NF-κB activation in cells with downregulated c-FLIP

(A) HeLa-CD95 cells stably downregulating c-FLIP were generated by RNA interference. HeLa-CD95 cells transfected with a control plasmid were used as control. Control HeLa-CD95 cells and c-FLIP-deficient HeLa-CD95 cells were stimulated with 1000 ng/ml anti-CD95 for the indicated time points. The lysates were used for western blot analysis against p-IκBα, c-FLIP and tubulin.

(B) Same as in (A) but with the addition of 20 μM zVAD-fmk 30 min prior to CD95 stimulation.

A

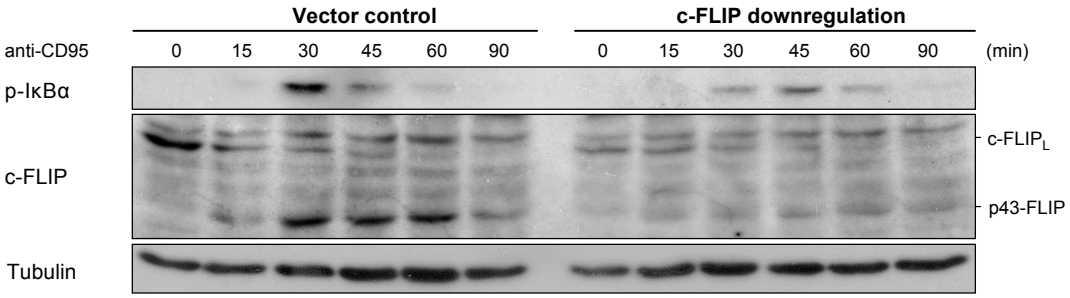

B

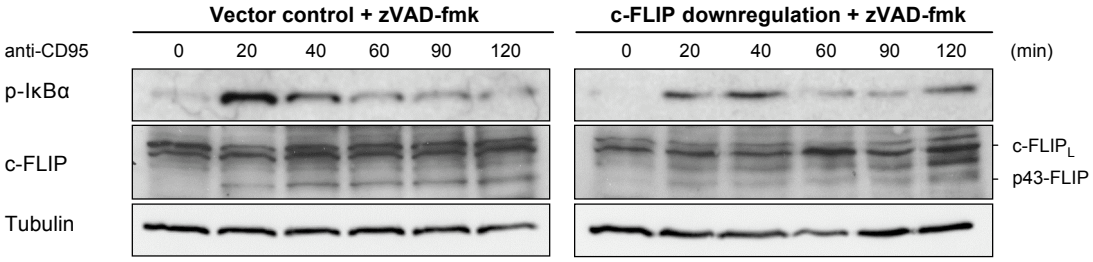

Figure S9. Impaired c-FLIP$_L$ processing

c-FLIP-deficient HeLa-CD95 cells were transiently transfected with 50 ng of c-FLIP$_L$ (left) or c-FLIP$_L$ (D376E) (right). Cells were stimulated with 1000 ng/ml anti-CD95 and processing of c-FLIP$_L$ to p43-FLIP was analyzed by western blot using antibodies against c-FLIP. Tubulin served as a loading control.